High Vacuum Gas Pumping and Boundary Coupling

Marco Cavenago
INFN/LNL, Laboratori Nazionali di Legnaro
viale dell'Universita' n. 2, I-35020 Legnaro (PD) Italy, cavenago@lnl.infn.it

Abstract:

The gas flow in the low pressure limit, named molecular flow regime, is a case of transport with zero viscosity. As an alternative to Monte Carlo methods typically used to estimate pipe conductance, an integral boundary equation (IBE) is here discussed, and solved, at least for simple 2D geometries (a circular junction and a simple pipe obstruction). An ad hoc algorithm to find obstacles on the view lines was developed for the latter case. The particular cares requested at the corners and in the interpolation from boundary to inner domain are shown. Relation between flow and pressures at ports is discussed, with the usual cosine law for the distribution of the velocities at input. For the circular junction, a typical PDE (partial differential equation) is here shown to have the same solution of the IBE, which allows for a comparison of the numerical precision of both approaches, showing a good agreement.

Keywords: molecular flow, gas pumping, integral equation

1 Introduction

Many scientific instruments are based on high vacuum equipment[1], with a gas pressure maintained in the order of 1 Pa or below by suitable pumps; ionization is possible, so that a plasma may be also formed. The gas pressure p in the vacuum chamber is of fundamental importance in all applications and depends on the size of the pipes connecting the vacuum chamber to the pumps. Two major regimes exists[2], depending on the Knudsen number K_n (ratio between geometry size D and mean free path λ): viscous ($K_n > 80$), which includes turbulent and laminar flow, and molecular ($K_n < 3$). Pressure p in the molecular regime is usually estimated by practical rules based on a lumped model of pipe conductances, which sometimes is a poor approximation for realistic shapes.

The case of viscous flow falls into the compressible Navier Stokes mode: with the decrease of p (and thus of K_n see Fig. 1) we first observe that simulation times lengthen due to the low values of viscosity used and then that convergence becomes impossible.

Molecular flow, where collisions between particles are neglected, put wall collisions in the foreground: the formulation as boundary coupled integral equation (IBE) is immediately apparent. Up to now, difficulties of their solution has limited practical use of this approach to the classical 1D applications of a circular straight tube[3, 4], with some recent generalization to conical tubes[5]. For more complicate shapes, Monte Carlo simulations of molecule collisions with chamber walls (with their precision issues) were the standard computational tools[6]: angular distribution of the gas molecules incoming from pipe openings was assumed to a be cosine law (consistently with the long pipe result), which happens to be equal to the distribution of gas rebouncing from walls. Symmetry conditions (useful in several cases) and generalization of the cosine law will require further discussion.

Here we present a general 2D model with integral boundary equation (next section), and its numerical solution for two simple geometries: a circular junction, a simple obstruction in a pipe (following sections). For the circular junction, the integral boundary equation for p is equivalent to a differential equation on the boundary for the incident pressure p^{in} (which is much faster to solve). Final model with Comsol Multiphysics include two boundary modes (for comparing p and p^{in}) and two ODE modes[7] to match the incoming flow. For the pipe obstruction, viewing factor calculation is carefully

optimized with some scripting. Remarks on the generalization to 3D are discussed in the conclusion.

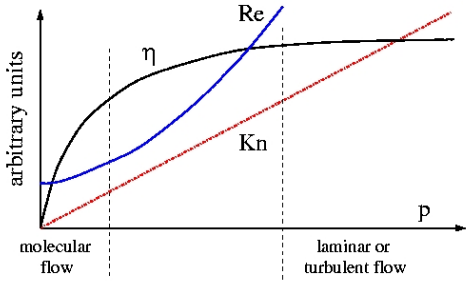

Figure 1: Sketch of viscosity (arbitrary units), Reynolds number R_e and Knudsen number K_n vs pressure p

2 Molecular flow

The well known ideal gas law $p = nk_BT$ relates the isotropic pressure of a gas to the number density of molecules n and to the temperature T, so that the mean free path

$$\lambda = \frac{1}{\sqrt{2}\, n\sigma} = \frac{k_BT}{\sqrt{2}p\sigma} \qquad (1)$$

is inversely proportional to the pressure; here σ is the cross section of elastic collision between molecules of mass m. The mass density is $\rho = n\, m = p\, m/k_BT$.

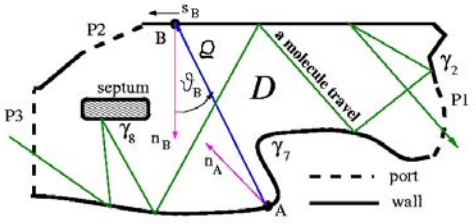

Figure 2: A generic planar geometry (if a septum exists, this is excluded from the simulation domain D). The point B is the running integration point, while A is the so-called destination or observation point

The average value of the modulus of the velocity $v_{av} = (8k_BT/\pi m)^{1/2}$ is of course different from the fluid velocity $\mathbf{v}_f$, which is the average of velocities; roughly $|\mathbf{v}_f| \le v_{av}$.

When $\lambda \ll D$, where D is a typical diameter of our pipe, the gas moves as a fluid, according to the compressible Navier Stokes equations (since mass density is proportional to pressure), with a fluid velocity $\mathbf{v}_f$ and a viscosity

$$\eta = c_3\rho\lambda v_{av} = 2^{-1/2}c_3 m v_{av}/\sigma \qquad (2)$$

here $c_3 = 0.499$ according to detailed transport calculation [8]; note η is indipendent from p in this regime.

When $\lambda \ge D/3$, the pipe wall perturb most of the gas motion, so that λ must be replaced by c_4D in equation (2), with the estimate $c_4 \cong 0.5$. Viscosity has to decrease with pressure $p \to 0$. Figure 1 shows a sketch of the dependence from p of η and of the well known Reynolds number $R_e = \rho\, v_f D/\eta$, which has the limit $v_f/c_3c_4v_{av} \cong 1$ for $p \to 0$.

Let us restrict to a 2D planar geometry as in Fig 2, where the simulation domain $\mathcal{D}$ (closed, but necessarily simply connected or convex) has solid walls and pipe openings (Fig 3) as boundaries; for simplicity we will not here discuss periodicity and/or symmetric boundary conditions. At equilibrium, the (numeric) flow density F^{in} of particles incident onto a wall

$$F^{\text{in}} = nv_{av}/4 = p^{\text{in}}/(2\pi m k_BT) \qquad (3)$$

is related to the pressure p^{in} incident on the wall; in the following we will convert flows to pressures by this proportion.

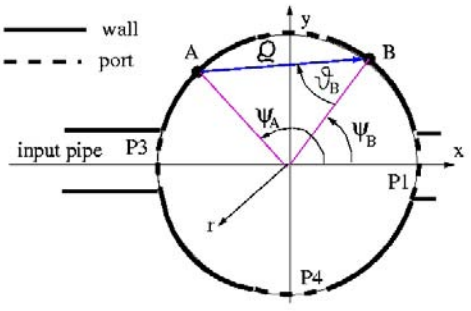

Figure 3: The example of a circular junction

At any point B on a solid wall, we assume that the reemitted numeric flow F^{re} is equal to F^{in}, and particle angular distibution is $f(\vartheta_B) = \frac{1}{2}\cos\vartheta_B$ where ϑ_B is the angle from the inward normal $\mathbf{n}_B$ to the particle direction (Fig 2). Let F^{vo} the net volumetric flow density (measured in [Pa m/s]) which enters from an opening; we assume that the flow reeemitted F^{re} is equal to F^{in}

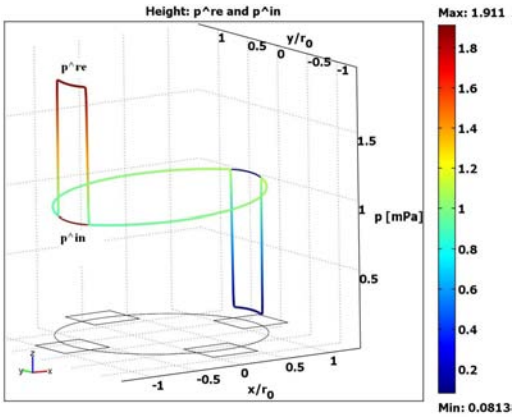

Figure 4: Elevation plot of simulation result for $p^{\rm re}$ and $p^{\rm in}$ with $p_0 = f_1 = 1$ mPa

with the shorthand $F^{ins} = 4F^{\rm vo}/v_{av}$ are the basic relation of particle conservation. plus the entering flow $F^{\rm vo}/k_BT$. The equivalent equations

$$F^{\rm re} = \frac{F^{\rm vo}}{k_BT} + F^{\rm in} \quad \text{and} \quad p^{\rm re} = F^{ins} + p^{\rm in} \quad (4)$$

Noting that any particle reemitted from point B will incide at a point A, making an angle ϑ_A with the inward normal $\mathbf{n}_A$, the incident pressure is

$$p^{\rm in}_A = \mathcal{L}[p^{\rm re}] = \int {\rm d}s_B \frac{\cos\vartheta_B \cos\vartheta_A}{2\varrho} p^{\rm re}_B I_{AB} \quad (5)$$

where the chord $\varrho = \mathbf{x}_B - \mathbf{x}_A$ is the vector from A to B and I_{AB} is the viewing indicatrix: equal to one if line segment AB is not obstructed (by walls), otherwise equal to zero. In particular, $I_{AB} = 0$ if $\cos\vartheta_B < 0$ or if $\cos\vartheta_A < 0$, since these cases corrispond to a chord passing into the walls.

Equations (4) and (5) are a formulation of our problem with integral boundary equation (IBE) only; references the pressure

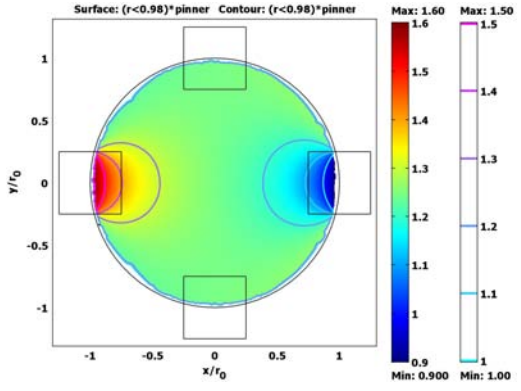

Figure 5: Simulation results: contour and surface plot of p^i (note the $r < 0.98 r_0$ mask) ; Here $p_3 = 2$ mPa and $p_1 = 0.5$ mPa, with the result $f_1 = 0.825$ mPa and $p_0 = 1.25$ mPa

inside $\mathcal{D}$ is not necessary; anyway for post-processing we define the inner (or isotropic) pressure at an inner point A as

$$p^i_A = \mathcal{M}[p^{\rm re}] = \int {\rm d}s_B \frac{\cos\vartheta_B}{2\pi\varrho} p^{\rm re}_B I_{AB} \quad (6)$$

this can be justified by balancing the in and out flows on a circle of radius $\epsilon \cong h$ centered at A, where h is the mesh element size; so that eq. (6) holds strictly when distance w_A of A from walls is large enough:

$$w_A \equiv \min_B \varrho \geq h(A) \quad (7)$$

3 The circular junction

In the geometry of Fig 3, the simulation domain $\mathcal{D}$ is the circle $r \leq r_0$; let (ψ, r) be the polar coordinates and the output port P1 be around $\psi = 0$, while gas may enter from the other three ports. All points of the boundary γ see each other, so $I_{AB} = 1$; moreover $\cos\vartheta_B = \sin(|\psi_A - \psi_B|/2)$ from simple geometry, so that $\mathcal{L}$ simplifies to

$$\mathcal{L}[p^{\rm re}] = \tfrac{1}{4}\int_{-\pi}^{\pi} d\psi_B \, p^{\rm re}_B \sin(\tfrac{1}{2}|\psi_A - \psi_B|) \quad (8)$$

The expression (8) is directly implemented as boundary integration variable ('elle') in Comsol Multiphysics, with destination domain the boundary γ itself (here ψ_A is the destination coordinate). The boundary weak term looks like

```
bnd.expr='test(p)*(elle+fins-p)'
```

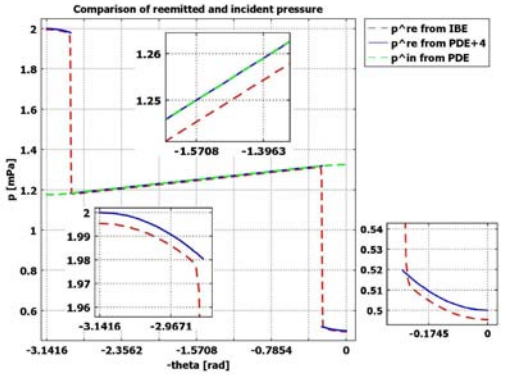

Figure 6: Simulation results on the lower boundary: $p^{\rm re}$ as computed from the IBE eq (8); $p^{\rm re}$ from eq. (4), with $p^{\rm in}$ computed from the PDE equation (10).

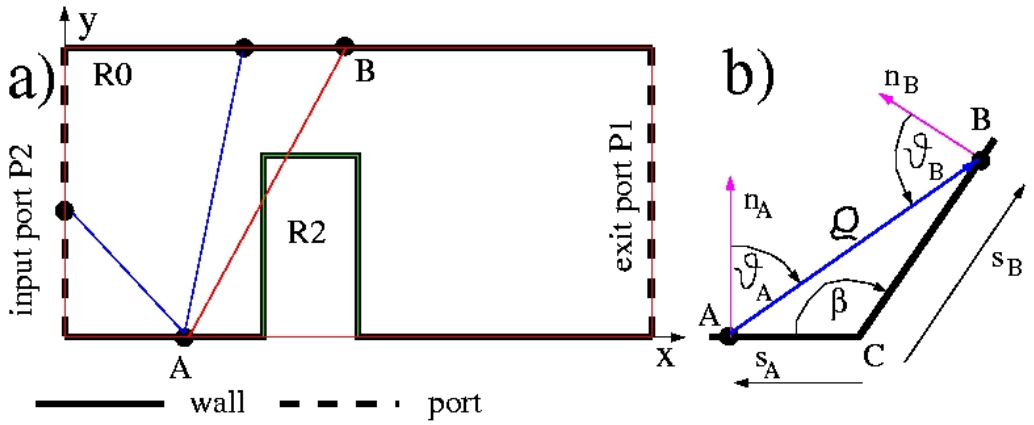

Figure 7: a) The simple obstruction, with a $I_{AB} = 0$ ray in red; b) a detail of a corner

where the $p^{\rm re}$ variable is typed 'p'. A first example of solution for the case $F^{ins} = f_1 = 1$ mPa (millipascal) on port 3 (near $\psi = -\pi$) and $F_{ins} = -f_1$ on port 1 is shown in figure 4. Ports 2 and 4 are here unused and we set the pressure reference value $p^{\rm re} = p_0 = 1$ mPa at $\psi = -\pi/2$.

It should be observed that the input pressure p_3 and exit pressure p_1 are usually given, while f_1 is the quantity to be computed. We thus add two ODE variables f_1 and p_0 to the multiphysics model; the two ODE equations are a linear combinations of the conditions $p^{\rm re}(-\pi) = p_3$ and $p^{\rm re}(\psi = 0) = p_1$. As another improvement, we specify a flow $F^{\rm ins} = -f_1 \cos\psi$ (on port 1 and 3) to better represent an uniform input flow in the x direction and its projection on the curved boundaries P1 and P3.

The surface plot of p^i of fig 5 reveals a good accuracy for $r/r_0 < 0.98$, with values showing that p^i does not have $p^{\rm re}$ as a limit value. To see reason of it, let us use a Fourier expansion

$$p^{\rm re} = p_0 \quad + \quad \sum_{m=1} [p^{\rm re}_m \cos(m\psi) + \quad p^s_m \sin(m\psi)] \, (r/r_0)^m \quad (9)$$

(the sin part is missing in our example, since we choose to use ports P1 and P3 only). We numerically note that $\mathcal{M}(1) = 1$ and $\mathcal{M}(r^m \cos m\psi) = \frac{1}{2} r^m \cos m\psi$ (and similarly for the sin part). This shows: 1) $\triangle p^i = 0$ and 2) the limit of p^i is $p_0 + \frac{1}{2}(p^{\rm re} - p_0)$. These facts are related to the Cauchy integral formula.

Generalization of these concepts to speed up computation in a generic geometry is being investigated, but another interesting equivalence should be noted for the circular junction (only). Since

$$\mathcal{L}[\cos(m\psi)] = \cos(m\psi)/(1 - 4m^2)$$

(as we verified numerically for $m = 0, 1, .., 4$), transforming equations (4) and (8) in Fourier cosine components, we get

$$-4m^2 p^{\rm in}_m = F^{ins}_m \quad \Leftrightarrow \quad \frac{\partial^2 p^{\rm in}}{\partial \psi^2} = F^{ins} \quad (10)$$

which can be easily implemented into a PDE weak boundary mode. To compare with previos example the the end conditions are $p^{\rm in}(-\pi) = p_3 - f_1$ and $p^{\rm in}(0) = p_3 + f_1$. Solution of equations (8) and (10) are compared in Fig 6 and they perfectly match. Equation (10) shows also that integral of F^{ins} is zero. Note that p_0 assumes the value $\frac{1}{2}(p_1 + p_3)$ in the result, that is the average pressure in the domain.

4 The simple obstruction

The simple obstruction model shown in Fig 7 has two ports, input P2 is the line segment $x = 0$, $0 \le x < L_y = 8$ mm and exit P1 is at $x = L_x = 1.6$ cm. In this example we specify directly that the pressure $p^{\rm re}(0, y)$ is a constant p_2 at P2, instead of assuming an uniform flow (presence of the obstruction is expected to produced non uniformity both of F^{ins} and of $p^{\rm in}$).

A new features is the presence of straight lines and of corners. Note the possible $1/\varrho$ singularity in the integrand of the eq (5) when $B \to A$. In the case A and B stay on the

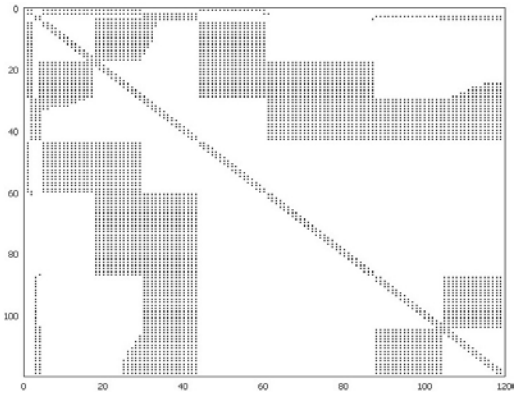

Figure 8: The stiffness matrix (full model has 314 nodes, but a 157 node model is shown here. Note linear Lagrange element were used for hystorical reason, and that port nodes (where p^{re} is given) are excluded from the shown stiffness matrix

same line segment, $\cos\theta_A = \cos\theta_B = 0$, so that this whole segment can be excluded from integration on B; this explains the gaps in the stiffness matrix of the problem shown in fig 8. In the case A and B stay on the same arc with curvature k (as in the previous circle example), we get $\cos\theta_A \cong \cos\theta_B = 0 \cong \frac{1}{2}k\varrho$, which cancel the singularity, leaving an integrand $\propto \varrho$. When A is at a fixed distance r_A near a corner C (with an angle $\beta < \pi$) and B moves on the other side of the corner, rapid variations of the integrand are observed. In lack of an absolutely certain formula (see appendix) to correct for the possible discontinuity of the integral (5) when A is within one mesh size from a corner C, it is advisable to refine the mesh as much as possible at corners.

In the case of angles $\beta > \pi$ the contribution of regions near the corner to the integral is zero (since the viewing factor is zero).

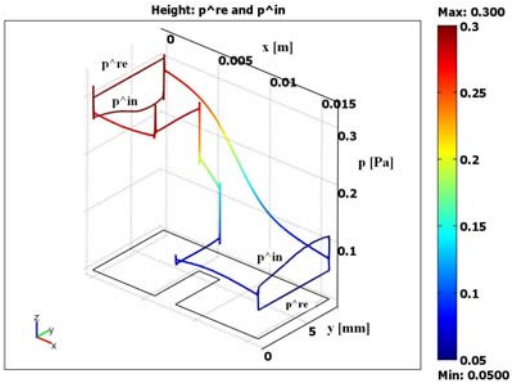

Figure 9: Elevation plot of simulation result for p^{re} and p^{in} with $p_2 = 0.3$ Pa and $p_1 = 50$ mPa

Conservatively we refine the mesh also at these corners, since they happen to be near to the obstruction region.

The computation of the viewing factor I_{AB} is the most consuming task of the whole computation, especially when surface plots of p^{i} are generated in the postprocessing. To speed up it, we observed that a ray from A to B can be stopped only by the small rectangle R2, see fig 7, since the big rectangle R0 is convex. Computing the intersection of the ray AB with the sides of R2 is fast, since they are parellel to x or y: before calling the `'femstatic'` solver a table is prepared, where the data for the rules to compute the intersections are stored, as a function of the indices of edges to which A and B belong.

An elevation view of reemitted pressure p^{re} is plotted in fig 9. Note the small spikes at the $\beta = \pi/2$ corners, as anticipated. We observe that their effects on the whole solution is very small (except near the corners), since the coupling is only via the integral (5). The large jump at the input and output port is not an error, but is to satisfy the boundary condition. Moreover, thanks to eq (4), the net flow density (in rescaled units) in the x-direction is $p_2 - p^{\mathrm{in}}$ at port 2 (input) and $p^{\mathrm{in}} - p_1$ at port P1 (exit); these are compared in figure 10.

A steep descent and a step of p^{re} are visible at the $\beta = 3\pi/2$ corners, in perfect analogy with the possible differences of illumination on two adjacent sides of a pilaster, as later explained. The elevation plot of p^i shown in fig 11 is smooth in the region given by equation (7).

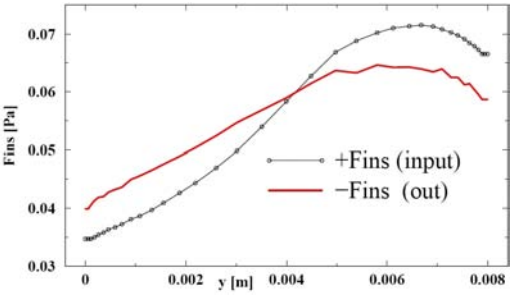

Figure 10: Input and exit flow density F^{ins} (here rescaled in Pa, to obtain the volumetric flow density F^{ins} multiply by $v_{av}/4 = 120$ m/s for nitrogen at $T = 300$ K); note that flow is still non-uniform due the obstuction

5 Conclusion and perspectives

The possibility to solve integral equation on boundary with finite elements methods allowed us to find the gas densities and flows in the molecular regime (a classical problem of physics and of technology), which great precision (as compared to usual Monte Carlo methods) almost everywhere in the solution domain. Implementation of integral equations in Comsol Multiphysics was seamless[7] and post-processing helped insight of elaborate mathematical objects. Since the ruling equation is not in the form of a partial differential equation (PDE), solution may include discontinuous features (especially at corners and borders of the domain). In general, in order to discriminate numerical noise from physical features, localized mesh refinements seem very effective. Simple techniques to speed up the viewing factor calculation were used.

In a simplified case, the ruling equation was found equivalent to a PDE, which allows for a very satisfying test of the solution precision. This line of investigation is worth of future investigations.

Among other works in progress, we are considering the possibility of openings where the tangential flow of particles is significant, generalizing the cosine law into

$$f(\vartheta) = p^{\mathrm{re}}(B)(\tfrac{1}{2}\cos\vartheta + c_5 \sin\vartheta) \qquad (11)$$

where c_5 is a small constant.

Generalization to elaborate 3D geometries may require improvements in the vieving factor calculation speed, but looks well possible, considering the similarity with the problem of surface illuminations in a room [9] and with the problem of high temperature radiative cooling[10]. These tasks can be helped by specialized radiosity algorithms[10], like the methods used in rendering a (texture mapped) scene. In the case of room illumination, wall reemission is smaller than incident light, so total input flow can be different from zero (and iterative solution methods naturally apply). In the case of radiative cooling, heat adsorbed of one surface can be reemitted from the other side. Use of PC graphical hardware for viewing factor calculation was sometimes suggested.

In some large accelerators, we typically find regions where 3D molecular flow calculation applies and others where Navier Stokes equation applies (larger diameter and/or larger pressure): capability of merging both approach appears extremely important.

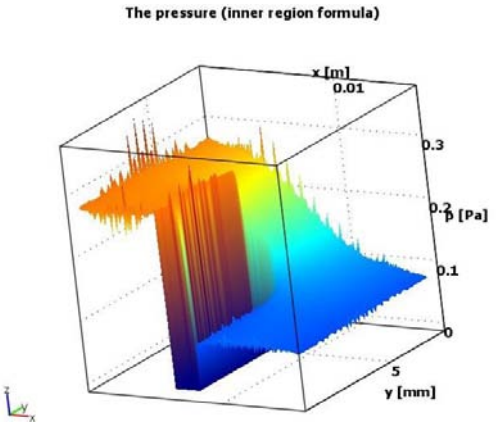

Figure 11: A surface plot of inner pressure p^{i}; spikes near the boundaries are due to the $1/\varrho$ singularity, see eq (7)

References

[1] H. F. Dylla "Development of ultrahigh and extreme high vacuum technology for physics research" J. Vac. Sci. Technol. A, **21**, S25 (2003)

[2] B. Ferrario, *Introduzione alla tecnologia del vuoto*, (ed. A. Calcatelli), Patron editore, Bologna (1999)

[3] P. Clausing "The flow of highly rarefied gases through tubes of arbitrary length" J. Vac. Sci. Technol. A **8**, 636 (1971)

[4] D. J. Santeler, "New concepts in molecular gas flow", J. Vac. Sci. Technol. A, **4**, 338 (1986)

[5] B. Mercier "Conductance measurement of a conical tube and calculation of the pressure distribution" J. Vac. Sci. Technol. A **24**, 529 (2006)

[6] D. H. Davis "Monte Carlo calculation of molecular flow rates through a cylindrical elbow and pipes of other shapes", J. Appl. Phys. **31**, 1169 (1960)

[7] W. B. Zimmerman, *Multiphysics modelling with finite element methods*, Singapore, World Scientific, (2006).

[8] S. Chapman, Proc. Roy. Soc. London, A **177**, 38 (1940-11941)

[9] C. Goral, K. E. Torrance, D. P. Greenberg and B. Battaile, "Modeling the interaction of light between diffuse surfaces", Computer Graphics, **18**, 213 (1984)

[10] S. Mazumder, "Methods to Accelerate Ray Tracing in the Monte Carlo Method for Surface-to-Surface Radiation Transport", J. Heat Transfer, **128**, 945 (2006)

Appendix

To compute the contribution $\mathcal{L}_C$ of the edge portion near a corner C to the eq (5), let us call Λ the proper cut-off on the s_B integration variable (oriented as shown in fig 7.b) and note that $\cos\vartheta_B = s_A \sin(\beta)/\varrho$; similarly for ϑ_A. We get

$$\mathcal{L}_C(\beta, s_A, \Lambda) = \int_0^\Lambda \mathrm{d}s_B p_B^{\mathrm{re}} \frac{s_B s_A (\sin\beta)^2}{2\varrho^3} \tag{12}$$

with $\varrho = (s_A^2 + s_B^2 - 2\, s_A s_B \cos\beta)^{1/2}$. Note that $p_B^{\mathrm{re}} \cong p_C^{\mathrm{re}}$ suffices for a first estimate. A large overestimate is obtained by taking formally $\Lambda \to \infty$ so that

$$\mathcal{L}_C < \mathcal{L}_C(\beta, s_A, \infty) = p_C^{\mathrm{re}}\, g_1(\beta) \tag{13}$$

with $g_1(\beta) = \frac{1}{2}(1 + \cos\beta)$ which proves that $\mathcal{L}_C$ is bounded (at least, it is not infinite). A more strict estimate may come from a simmetric corner cut-off $s_B \le s_A$ which gives

$$\mathcal{L}_C \cong \mathcal{L}_C(\beta, s_A, s_A) = p_C^{\mathrm{re}}\, g(\beta) \tag{14}$$

with $g(\beta) = \frac{1}{2}(1 - \sin(\beta/2))$. This finite contribution is correctly estimated by the boundary integration when $A \neq C$; but when $A = C$ a literal application of equation (5) or (12) gives $\mathcal{L}_C = 0$. We speculate that the inclusion (in future calculations) of a point contribution (as a point weak term) like equation (13) [or better (14)] may help precision in the case $A = C$ (that is, at corners).